5. Techniques for Surface Chemical Composition

To obtain a complete description of surface, need elemental or molecular composition in addition to structural information

Many composition sensitive techniques based on *electron spectroscopy*

- use electrons as incident or detected particle
- exploit surface sensitivity of low energy electrons

5.1 Electron Spectroscopy and Surface Sensitivity

Distance electron can travel in solid depends on (i) material and (ii) electron KE

Measure attenuation of electrons by covering surface with known thickness of element

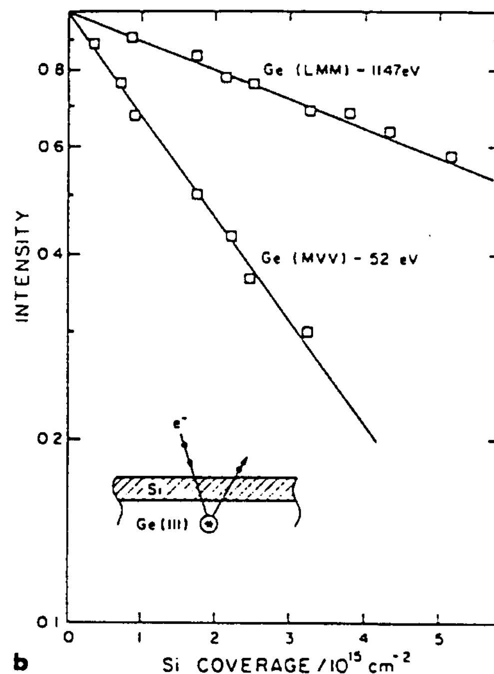

Loss processes (*inelastic scattering*) reduce KE and can prevent escape from surface:

Phonon excitation - collective excitation of atoms in unit cell (0.01-10 eV)

Plasmon excitation - collective excitation of electrons (5-20 eV)

Interband transitions, *ionization*

Measure attenuation lengths for various materials and KE's:

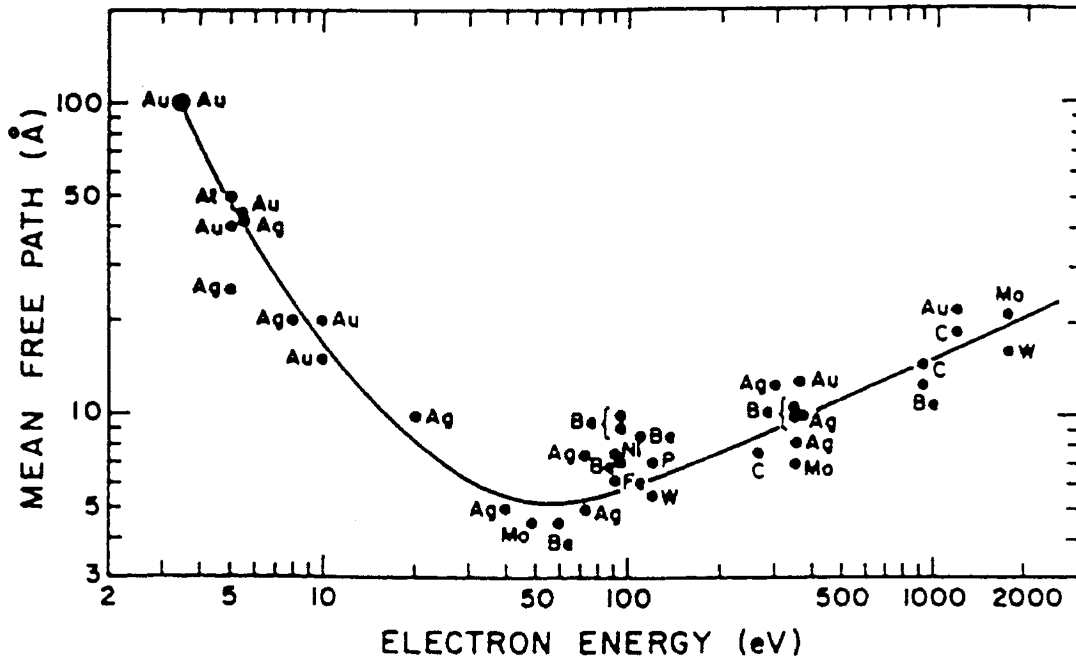

"Universal curve" of electron *inelastic mean free path* (IMFP) versus KE (eV)

IMFP is average distance between inelastic collisions (Å)

Minimum of ~ 5-10 Å for KE ~ 50-100 eV - *maximum surface sensitivity*

General Classification of Electron Spectroscopic Methods:

Method	Particle In	Particle Out	Information	Technique
Photoemission	Photon	Electron	Filled core states	XPS
Photoemission	Photon	Electron	Filled valence states	UPS
Inverse photoemission	Electron	Photon	Empty states	IPES
Electron energy loss	Electron	Electron	Electronic & vibrational transitions	EELS, HREELS
Auger	Electron	Electron	Filled states	AES
Absorption / emission*	Photon	Photon	Electronic transitions, filled states	UV-Vis, XRF

* not normally surface sensitive

5.2 X-ray Photoelectron Spectroscopy (XPS)

also known as *electron spectroscopy for chemical analysis* (ESCA)

Semi-quantitative technique for determining composition based on the photoelectric effect

5.2.1 The Photoemission Process

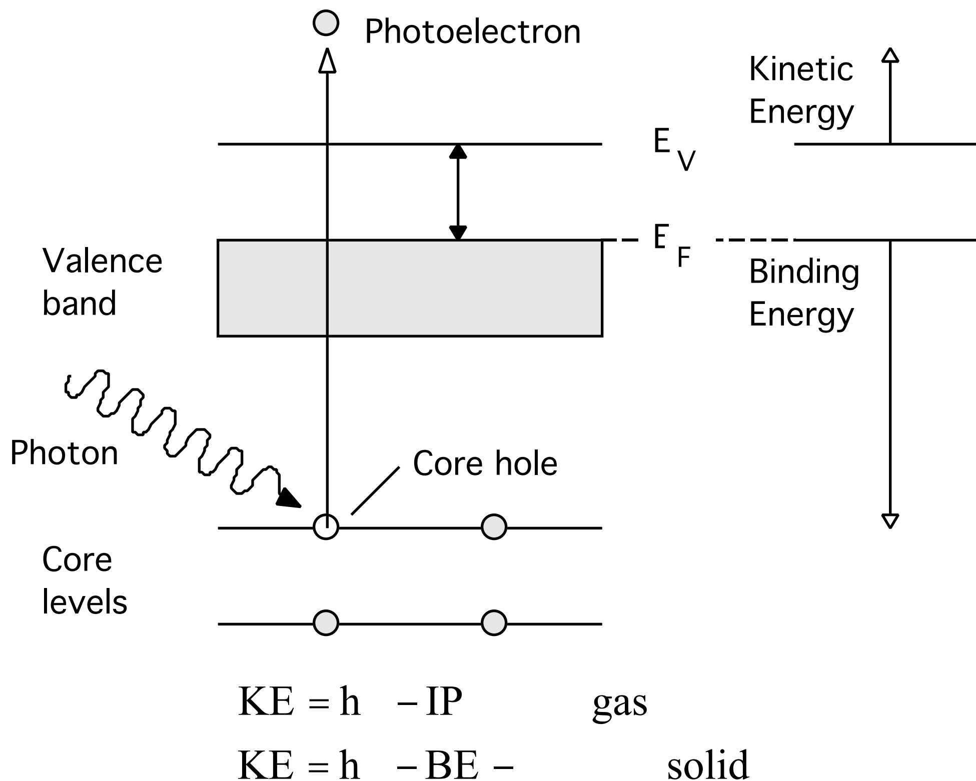

$KE = h \quad - IP$ gas

$KE = h \quad - BE -$ solid

Absorption very fast - ~10^{-16} s

Clearly from picture above,

- no photoemission for h <
- no photoemission from levels with BE + > h
- KE of photoelectron increases as BE decreases
- intensity of photoemission intensity of photons

- need monochromatic (x-ray) incident beam
- a range of KE's can be produced if valence band is broad
- since each element has unique set of core levels, KE's can be used to fingerprint element

Binding energy (BE) represents strength of interaction between electron (n, l, m, s) and nuclear charge

- in gases, BE   IP (n, l, m, s)
- BE follows energy of levels: BE(1s) > BE(2s) > BE(2p) > BE(3s)…
- BE of orbital increases with Z: BE(Na 1s) < BE(Mg 1s) < BE(Al 1s)…

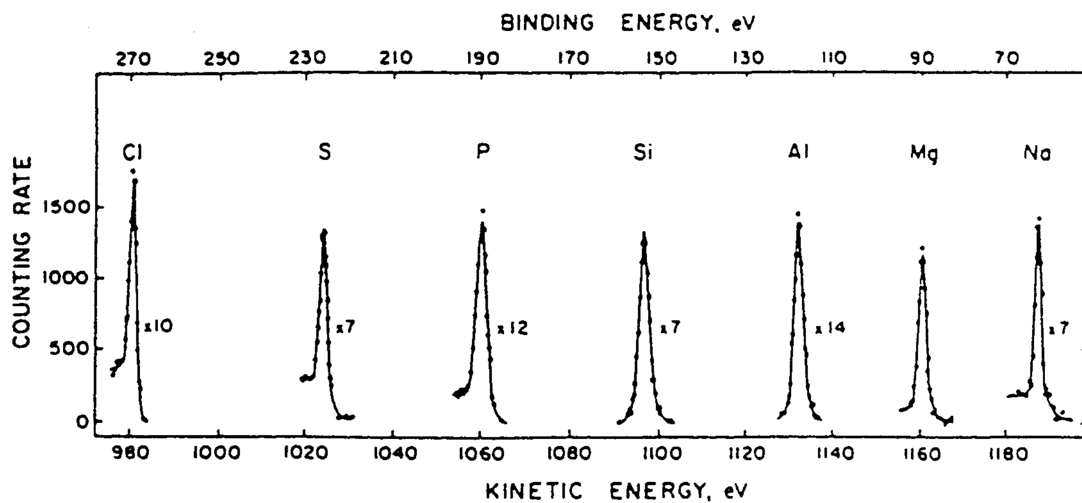

- BE of orbital not affected by isotopes: BE(^{7}Li 1s) = BE(^{6}Li 1s)

What is fate of core hole?

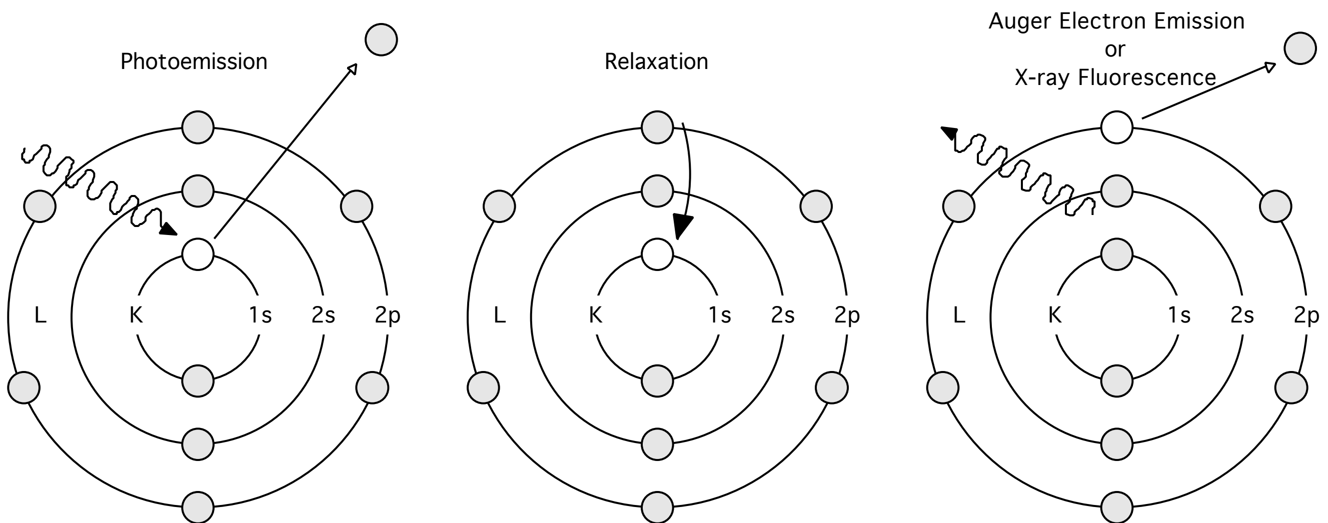

- Auger electron emission - basis of Auger electron spectroscopy (AES)
- X-ray fluorescence

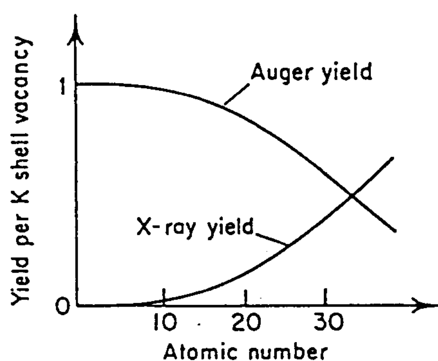

Fig. 44. The relative probabilities of X-ray emission and Auger electron emission in the decay of K (1s) holes in the lighter elements.

5.2.2 Koopman's Theorem

The BE of an electron is simply difference between initial state (atom with n electrons) and final state (atom with n-1 electrons (ion) and free photoelectron)

$$BE = E_{final}(n-1) - E_{initial}(n)$$

If no relaxation followed photoemission, BE = - orbital energy which can be calculated from Hartree-Fock

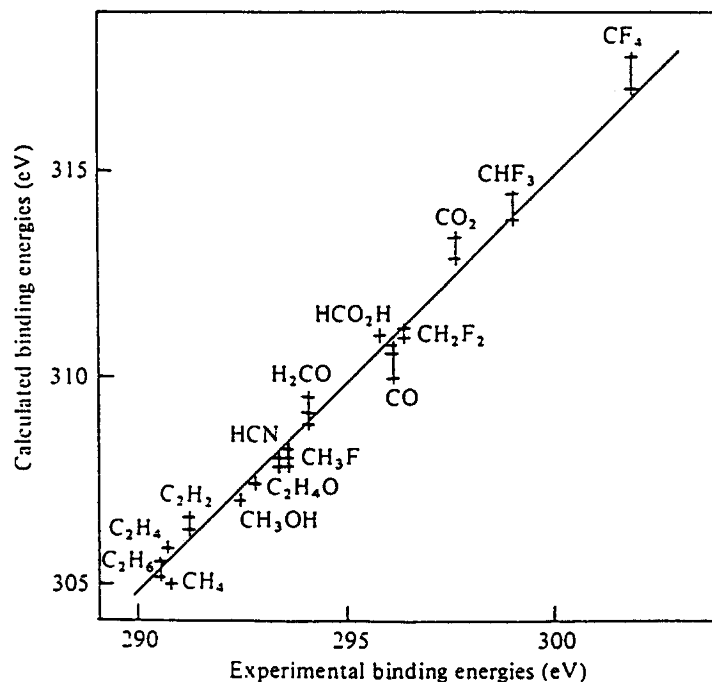

Fig. 3.13 Comparison of experimental XPS C 1s binding energies with those calculated via Koopman's theorem for C in a range of molecules. Although experimental and theoretical values differ by 15 eV (associated with relaxation effects) the systematic comparison is excellent as indicated by the straight line of unity gradient (after Shirley, 1973).

Measured BE's and calculated orbital energies different by 10-30 eV because of:

- electron rearrangement to shield core hole - the frozen orbital approximation is not accurate
- electron correlation (small)
- relativistic effects (small)

Really, both *initial state effects* and *final state effects* affect measured BE

5.3 Primary Structure in XPS

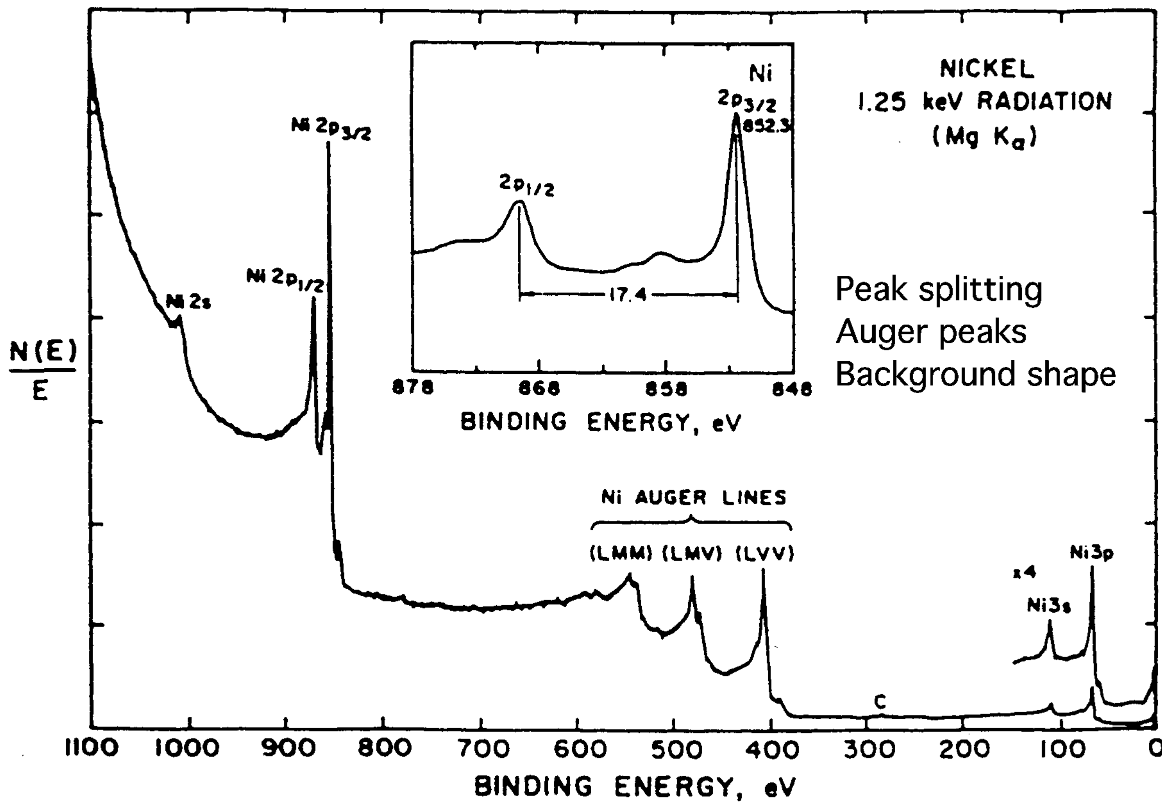

Photemission process often envisaged as three steps

(i) Absorption and ionization (initial state effects)

(ii) Response of atom and creation of photoelectron (final state effects)

(iii) Transport of electron to surface and escape (extrinsic losses)

All can contribute structure to XPS spectrum

5.3.1 Inelastic Background

XPS spectra show characteristic "stepped" background (intensity of background to high BE of photoemission peak is always greater than low BE)

Due to inelastic processes (extrinsic losses) from deep in bulk

> Only electrons close to surface can, on average, escape without energy loss
>
> Electrons deeper in surface loose energy and emerge with reduced KE, increased BE
>
> Electrons very deep in surface loose all energy and cannot escape

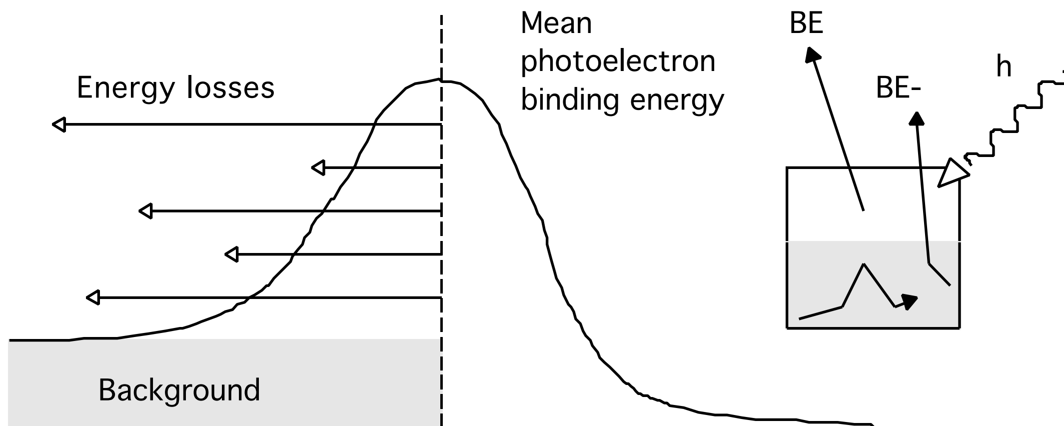

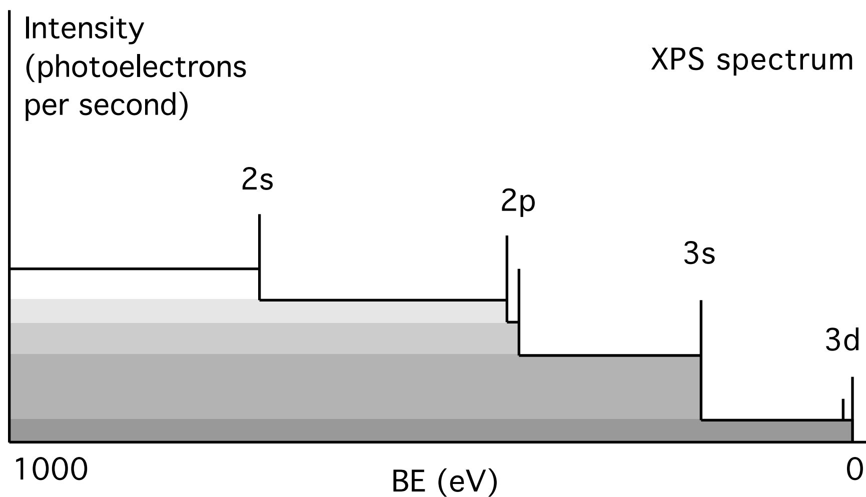

What is probability that electron of kinetic energy KE (and IMFP) will arrive at surface without energy loss?

- what is sampling depth d of photoelectron?

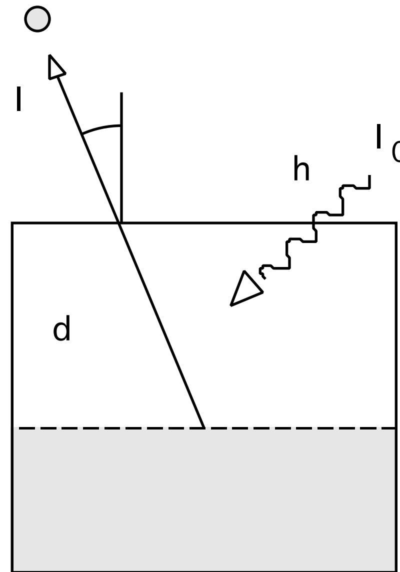

$$I = I_0 \exp \frac{-d}{\cos}$$

$$\ln \frac{I}{I_0} = \frac{-d}{\cos}$$

For normal takeoff angle, cos = 1

When d = , - $\ln(I/I_0)$ = 0.367 or 63.3 % of electrons come from within 1 of surface

When d = 2 , - $\ln(I/I_0)$ = 0.136 or 86.4 % of electrons come from within 2 of surface

When d = 3 , - $\ln(I/I_0)$ = 0.050 or 95.0 % of electrons come from within 3 of surface

5.3.2 Spin-Orbit Splitting (SOS)

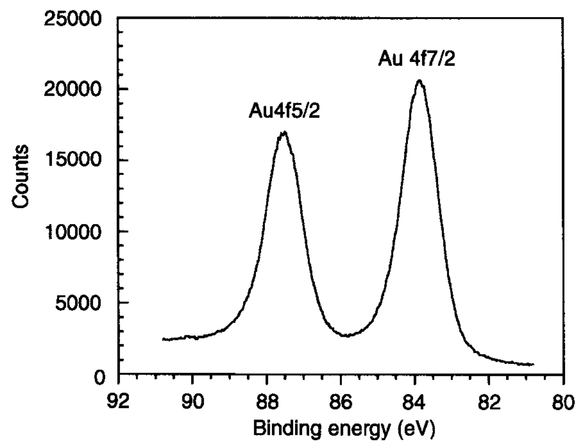

Figure 3.12. Spin-orbit coupling leads to a splitting of the 4f photoemission gold into two subpeaks

Spin-orbit splitting is an *initial state effect*

For any electron in orbital with orbital angular momentum, coupling between magnetic fields of spin (s) and angular momentum (l) occurs

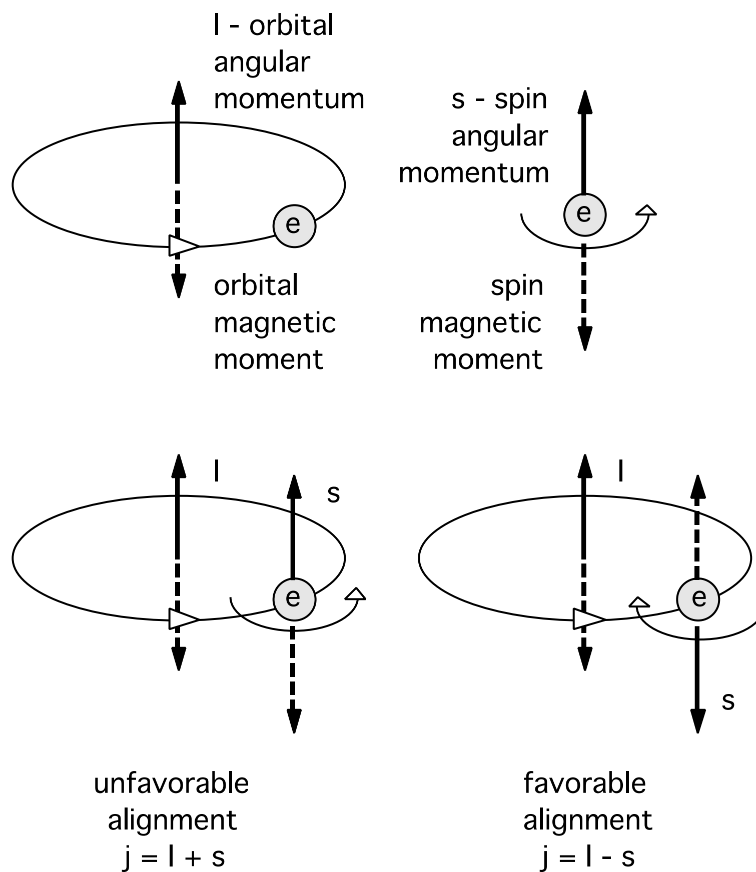

Total angular momentum $j = |l \pm s|$

Quantum numbers				Atomic notation	X-ray notation
n	l	s	j	$n\,l_j$	
1	0	± 1/2	1/2	$1s_{(1/2)}$	K_1
2	0	± 1/2	1/2	$2s_{(1/2)}$	L_1
2	1	+ 1/2	3/2	$2p_{3/2}$	L_2
2	1	- 1/2	1/2	$2p_{1/2}$	L_3
3	0	± 1/2	1/2	3s	M_1
3	1	- 1/2	1/2	$3p_{1/2}$	M_2
3	1	+ 1/2	3/2	$3p_{3/2}$	M_3
3	2	-1/2	3/2	$3d_{3/2}$	M_4
3	2	+ 1/2	5/2	$3d_{5/2}$	M_5

But how many spin-orbit split levels at each j value?

$$\text{Degeneracy} = 2j + 1$$

Subshell	j values	Degeneracy
s	1/2	-
p	1/2, 3/2	2, 4 = 1, 2
d	3/2, 5/2	4, 6 = 2, 3
f	5/2, 7/2	6, 8 = 3, 4

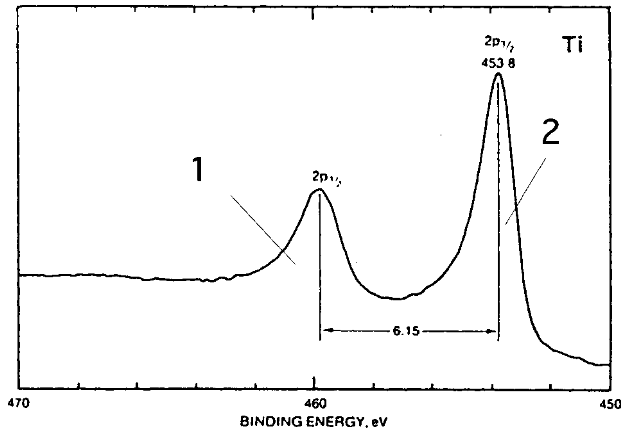

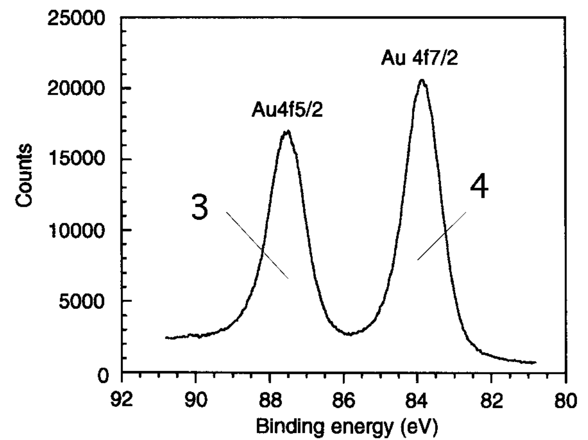

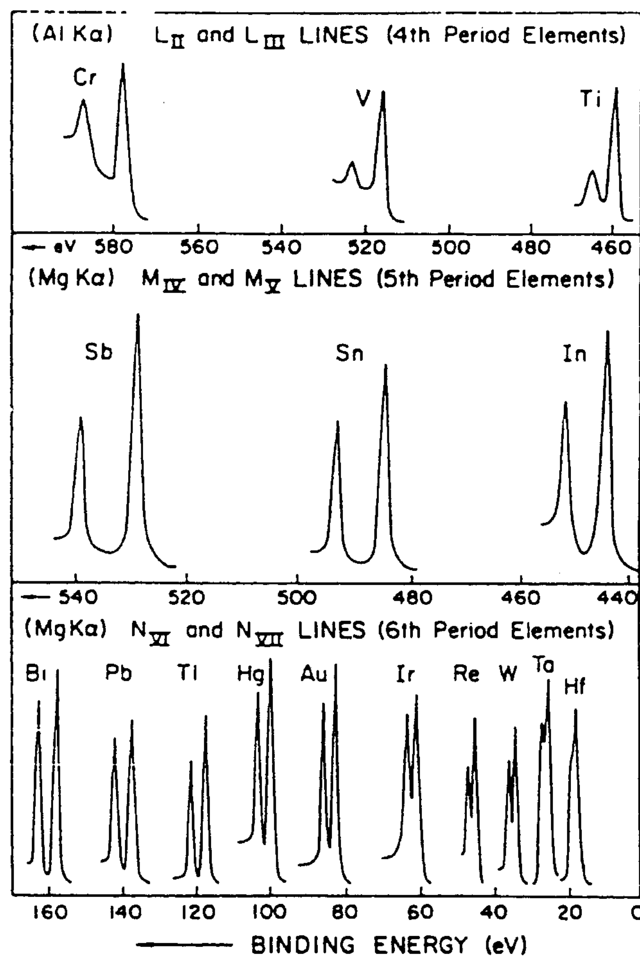

Observations:

- s orbitals are not spin-orbit split - singlet in XPS
- p, d, f… orbitals are spin-orbit split - doublets in XPS

- BE of lower j value in doublet is higher (BE $2p_{1/2}$ > BE $2p_{3/2}$)
- Magnitude of spin-orbit splitting increases with Z
- Magnitude of spin-orbit splitting decreases with distance from nucleus (increased nuclear shielding)

5.3.3 Auger Peaks

Result from excess energy of atom during relaxation (after core hole) creation

- always accompany XPS
- broader and more complex structure than photoemission peaks

KE independent of incident h

(will discuss in more detail later)

5.3.4 Core Level Chemical Shifts

Position of orbitals in atom is sensitive to chemical environment of atom

In gas phase, can see differences in core electron ionization energies:

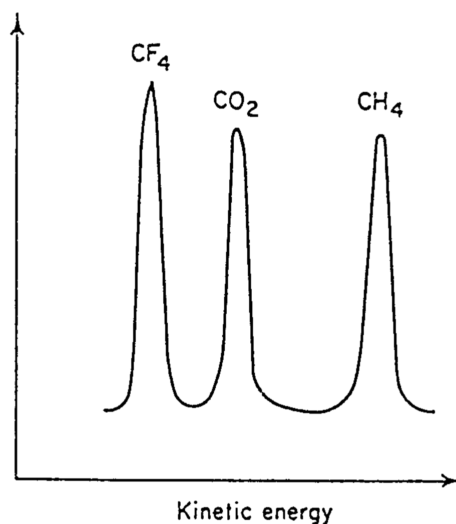

Fig. 53. The carbon 1s signals in the X-PE spectrum of an approximately equimolar gaseous mixture of CH_4, CO_2 and CF_4. (From Ref. 13.)

1s Ionization	Species	(eV)
B	IP (BF_3 - B_2H_6)	6.2
C	IP (CF_4 - CH_4)	11.1
N	IP (NF_3 - NH_3)	7.3
O	IP (O_2 - CH_3CHO)	5.5
F	IP (CF_4 - EtF)	3.2
S	IP (SF_6 - SH_2)	10.2

In solid all core levels for that atom shifted by approx. same amount (<10 eV)

Chemical shift correlated with *overall charge* on atom (Reduced charge increased BE)

(i) number of substituents

(ii) substituent electronegativity

(iii) formal oxidation state (unreliable depending upon ionicity/covalency of bonding)

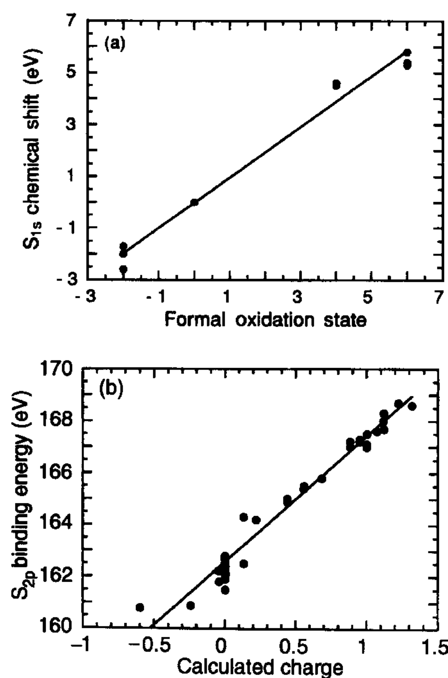

Figure 3.3. (a) The sulfur 1s chemical shifts, versus formal oxidation state for several inorganic sulfur species. (b) The sulfur 2p binding energy, versus calculated charge for several inorganic and organic sulfur species. Date taken from the results of Siegbahn *et al* [2]

Usually chemical shifts are thought of as initial state effect (i.e. relaxation processes are similar magnitude in all cases)

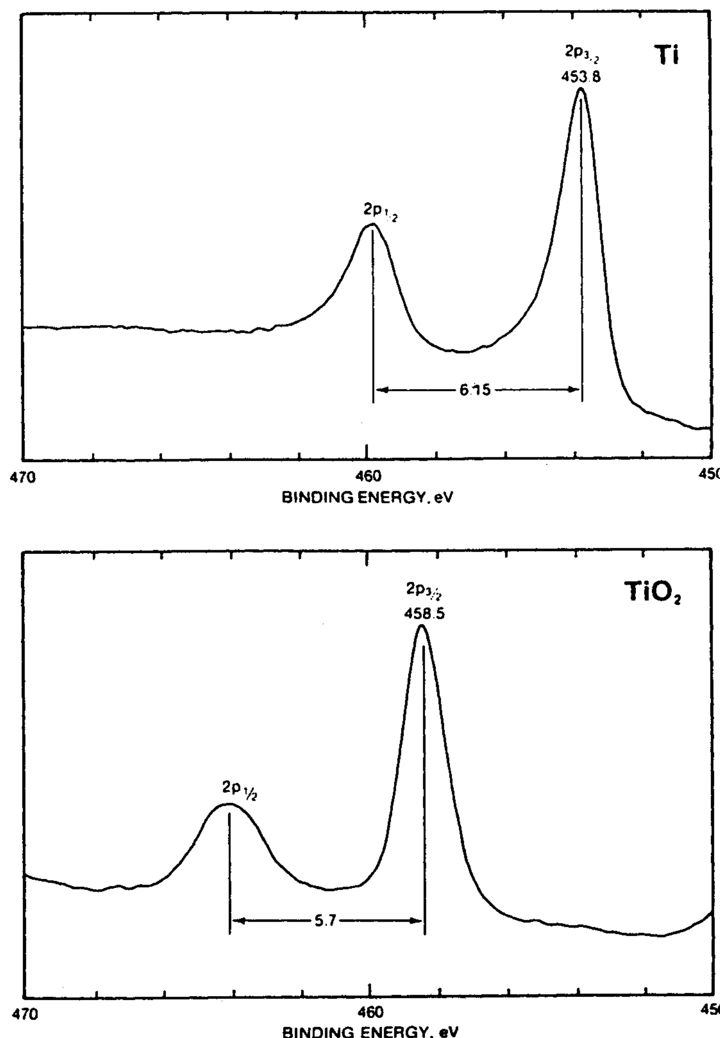

Ti $2p_{1/2}$ and $2p_{3/2}$ chemical shift for Ti and Ti^{4+}. Charge withdrawn Ti Ti^{4+} so 2p orbital relaxes to higher BE

Note: Spin-orbit splitting is approximately constant - confirming SOS is largely an initial state effect

Chemical shift information very powerful tool for functional group, chemical enviroment, oxidation state

Table 3.2. Typical C_{1s} binding energies for organic samples*

Functional group		Binding energy (eV)
hydrocarbon	C–H,C–C	285.0
amine	C–N	286.0
alcohol, ether	C–O–H, C–O–C	286.5
Cl bound to carbon	C–Cl	286.5
F bound to carbon	C–F	287.8
carbonyl	C=O	288.0
amide	N–C=O	288.2
acid, ester	O–C=O	289.0
urea	N–C(=O)–N	289.0
carbamate	O–C(=O)–N	289.6
carbonate	O–C(=O)–O	290.3
2F bound to carbon	$-CH_2CF_2-$	290.6
carbon in PTFE	$-CF_2CF_2-$	292.0
3F bound to carbon	$-CF_3$	293–294

*The observed binding energies will depend on the specific environment where the functional groups are located. Most ranges are ±0.2 eV, but some (e.g., fluorocarbon samples) can be larger

Table 3.3. Typical O_{1s} binding energies for organic samples*

Functional group		Binding energy (eV)
carbonyl	C=O, O–C=O	532.2
alcohol, ether	C–O–H, C–O–C	532.8
ester	C–O–C=O	533.7

*The observed binding energies will depend on the specific environment where the functional groups are located. Most ranges are ± 0.2 eV.

5.4 Secondary Structure in XPS

5.4.1 X-ray Satellites

In order to observe sharp photoemission lines in XPS, x-ray source must be monochromatic

X-ray emission in source based on x-ray fluorescence:

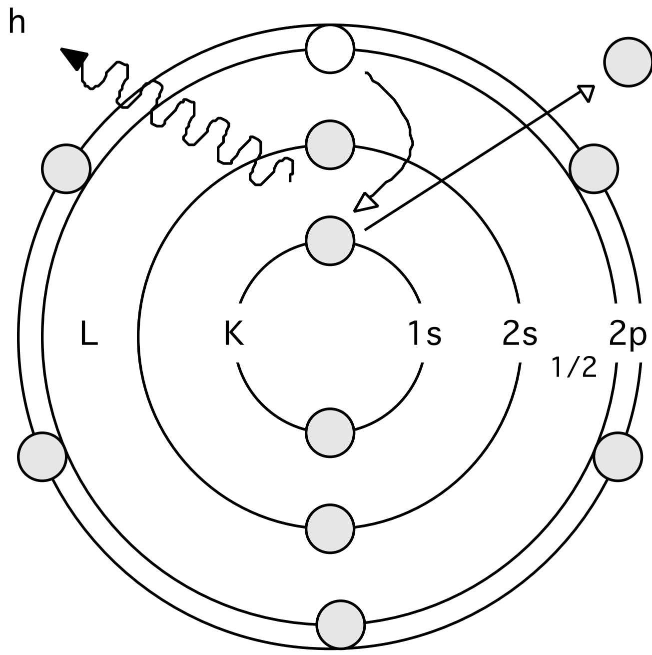

$2p_{3/2}$ 1s and $2p_{1/2}$ 1s transitions produce soft x-rays

$K_{1,2}$ radiation (unresolved doublet)

	h (eV)	FWHM (eV)
Mg	1253.6	0.7
Al	1486.6	0.85

Same transitions in doubly ionized Mg or Al produce $K_{3,4}$ lines at h ~ 9-10 eV higher…

3p 1s transitions produce K x-rays

X-ray source is usually unmonochromated so x-ray fluorescence emission lines superimposed on broad background (Bremsstrahlüng)

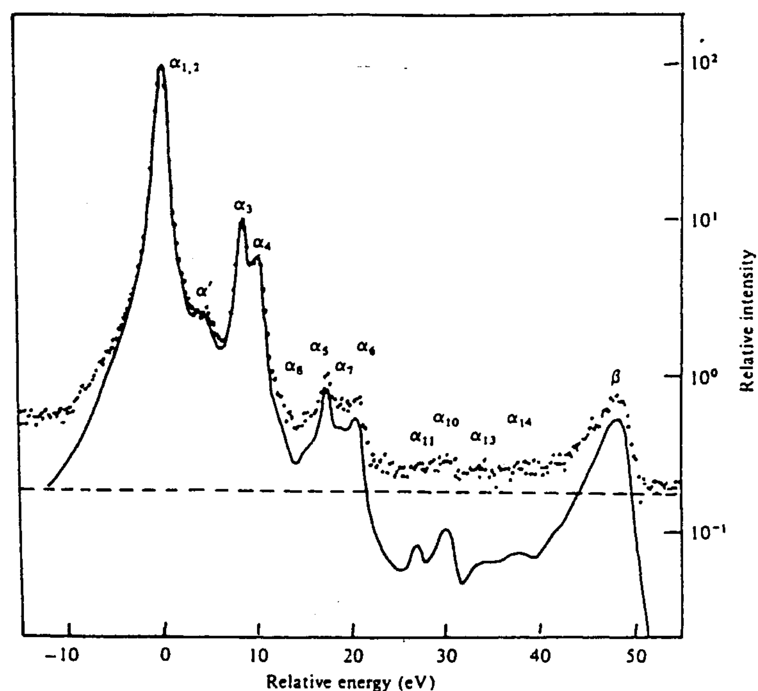

Emission from non-monochromatic x-ray sources produces "ghost" peaks in XPS spectrum at lower BE

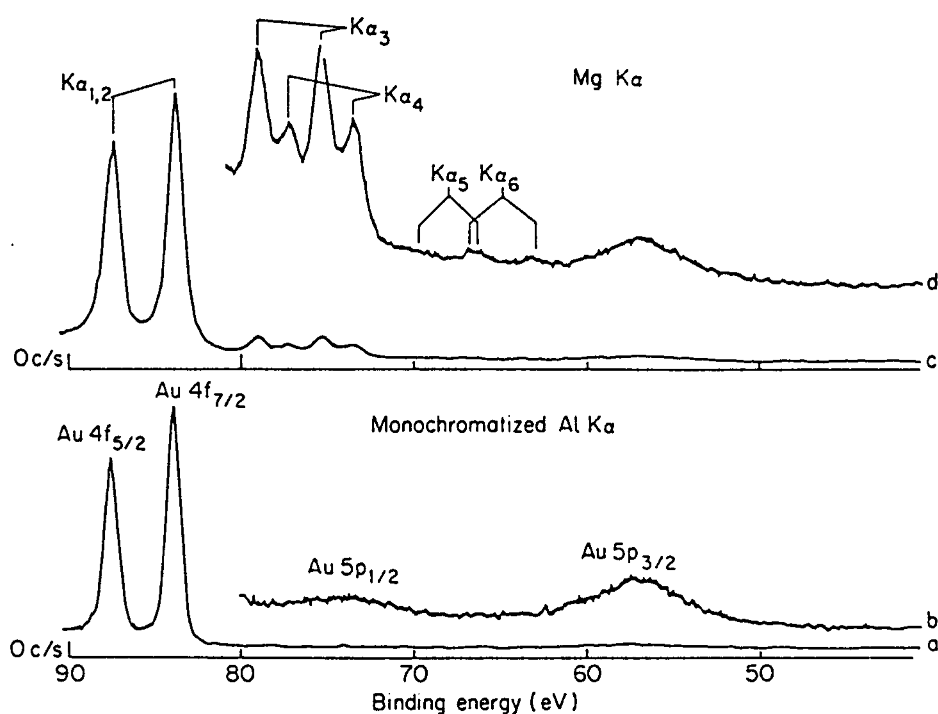

Fig. 4. Partial XP spectra of gold with and without monochromation of the X-rays. Upper spectra with Mg Kα (500 W), lower spectra with monochromatized Al Kα (900 W). Both scans have overall resolution of 0.95 eV f.w.h.m., 0.1 V s^{-1} scan speed, 0.33 s TC. Count rates are: (a) 10^4 counts s^{-1} f.s.d., (c) 3×10^4 counts s^{-1} f.s.d. (b) and (d) are $\times 10$ sensitivity.

5.4.2 Surface Charging

Electrical insulators cannot dissipate charge generated by photoemission process

Surface picks up excess *positive* charge - all peaks shift to *higher* BE

Can be reduced by exposing surface to neutralizing flux of low energy electrons - "flood gun" or "neutralizer"

BUT must have good *reference peak*

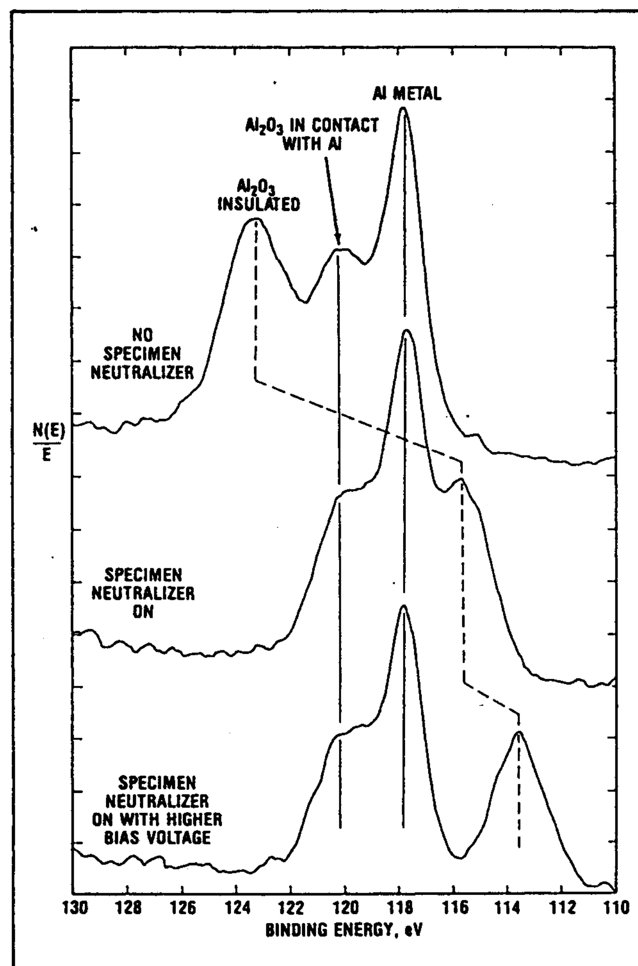

Figure 17. Use of specimen neutralizer to shift the partial spectrum from insulating domains (Al 2s lines from Al_2O_3 on aluminum sample).

5.4.3 Final State Effects (Intrinsic Satellites)

Final state effects arise during atom relaxation and creation of photoelectron following core-hole creation

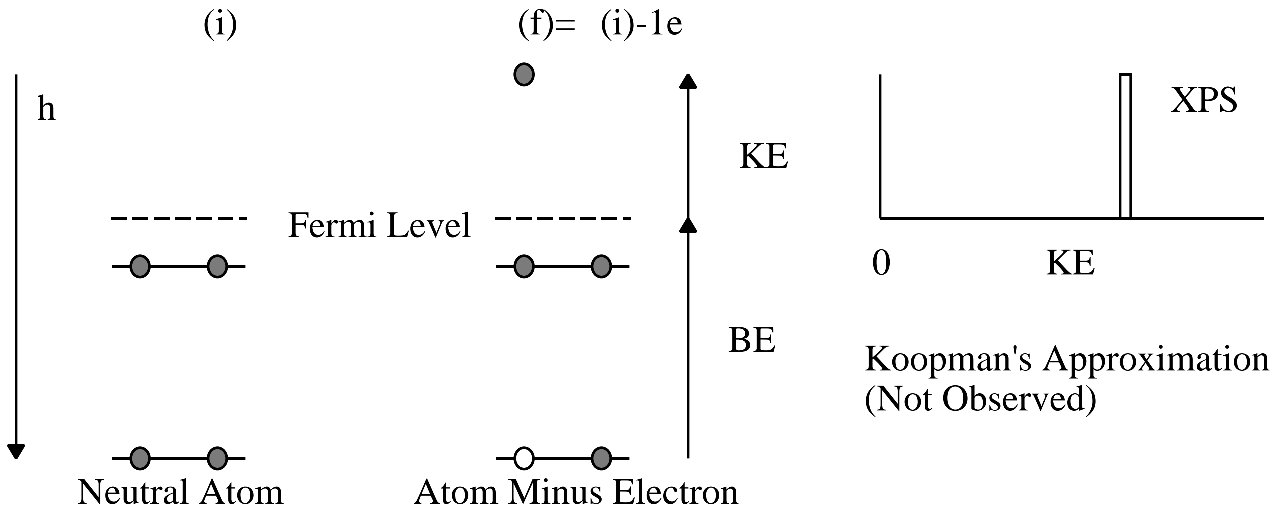

Koopman's energy never observed because of intra-atomic and interatomic screening by electrons

Solid relaxation shift

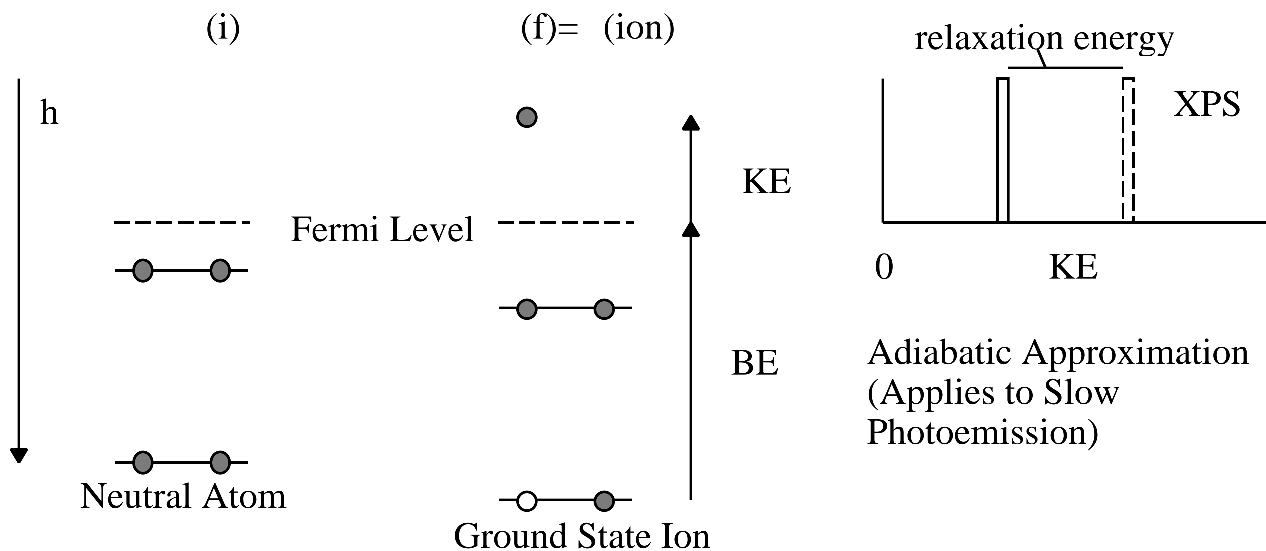

Adiabatic energy never observed because atom doesn't have enough time to *fully* relax to ground state ionic configuration before photoelectron is created

Photoelectron is created while ion is in various electronically excited states

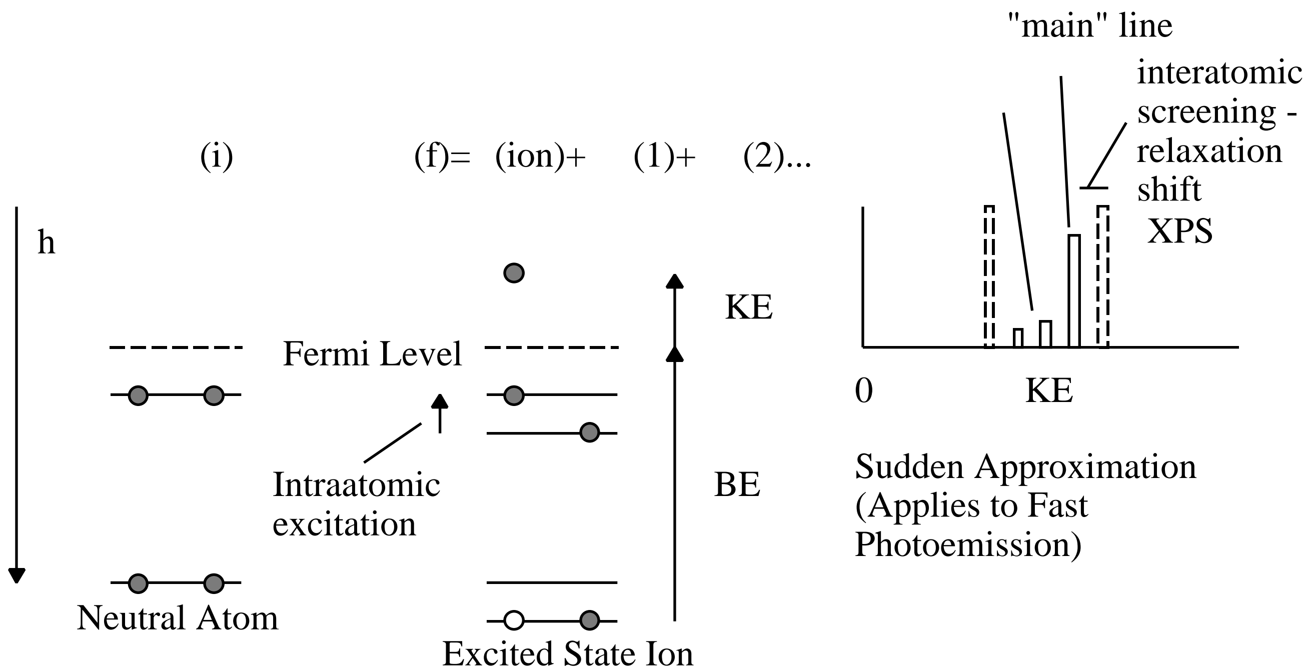

Energy of electronic excitation not available to departing photoelectron - satellites at lower KE, higher BE

- excitation of electron to bound state *shake-up satellite*
- excitation of electron to unbound (continuum) state *shake-off satellite*
- excitation of hole state *shake-down satellite* - rare

Longer excited states live more likely to see final state satellites

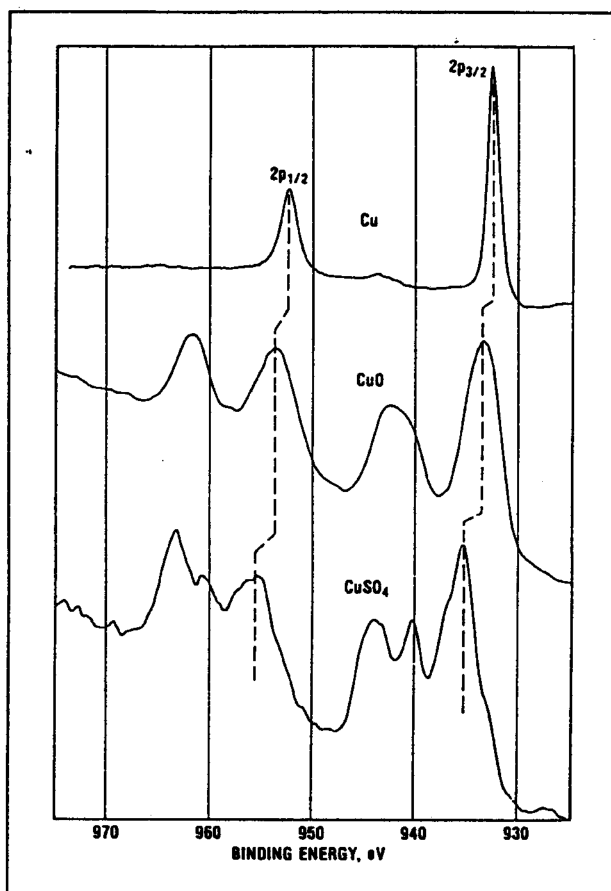

Figure 8. Examples of shake-up lines observed with the copper 2p spectrum.

Shake-up features especially common in transition metal oxides associated with paramagnetic species

Table 3 — General guide to paramagnetic species

Multiplet splitting and shake-up lines are generally expected in the paramagnetic states below.

Atomic No.	Paramagnetic States	Diamagnetic States
22	Ti^{+2}, Ti^{+3}	Ti^{+4}
23	V^{+2}, V^{+3}, V^{+4}	V^{+5}
24	Cr^{+2}, Cr^{+3}, Cr^{+4}, Cr^{+5}	Cr^{+6}
25	Mn^{+2}, Mn^{+3}, Mn^{+4}, Mn^{+5}	Mn^{+7}
26	Fe^{+2}, Fe^{+3}	$K_4Fe(CN)_6$, $Fe(CO)_4Br_2$
27	Co^{+2}, Co^{+3}	CoB, $Co(NO_2)_3(NH_3)_3$, $K_3Co(CN)_6$, $Co(NH_3)_6Cl_3$
28	Ni^{+2}	$K_2Ni(CN)_4$, square planar complexes
29	Cu^{+2}	Cu^{+1}
42	Mo^{+4}, Mo^{+5}	Mo^{+6}, MoS_2, $K_4Mo(CN)_8$
44	Ru^{+3}, Ru^{+4}, Ru^{+5}	Ru^{+2}
47	Ag^{+2}	Ag^{+1}
58	Ce^{+3}	Ce^{+4}
59-70	Pr, Nd, Sm, Eu, Gd, Tb, Dy, Ho, Er, Tm, Yb compounds	
74	W^{+4}, W^{+5}	W^{+6}, WO_2, WCl_4, WC, $K_4W(CN)_8$
75	Re^{+2}, Re^{+3}, Re^{+4}, Re^{+5}, Re^{+6}	Re^{+7}, ReO_3
76	Os^{+3}, Os^{+4}, Os^{+5}	Os^{+2}, Os^{+6}, Os^{+8}
77	Ir^{+4}	Ir^{+3}
92	U^{+3}, U^{+4}	U^{+6}

Has been used as fingerprint in polymer XPS (termed ESCALOSS by Barr)

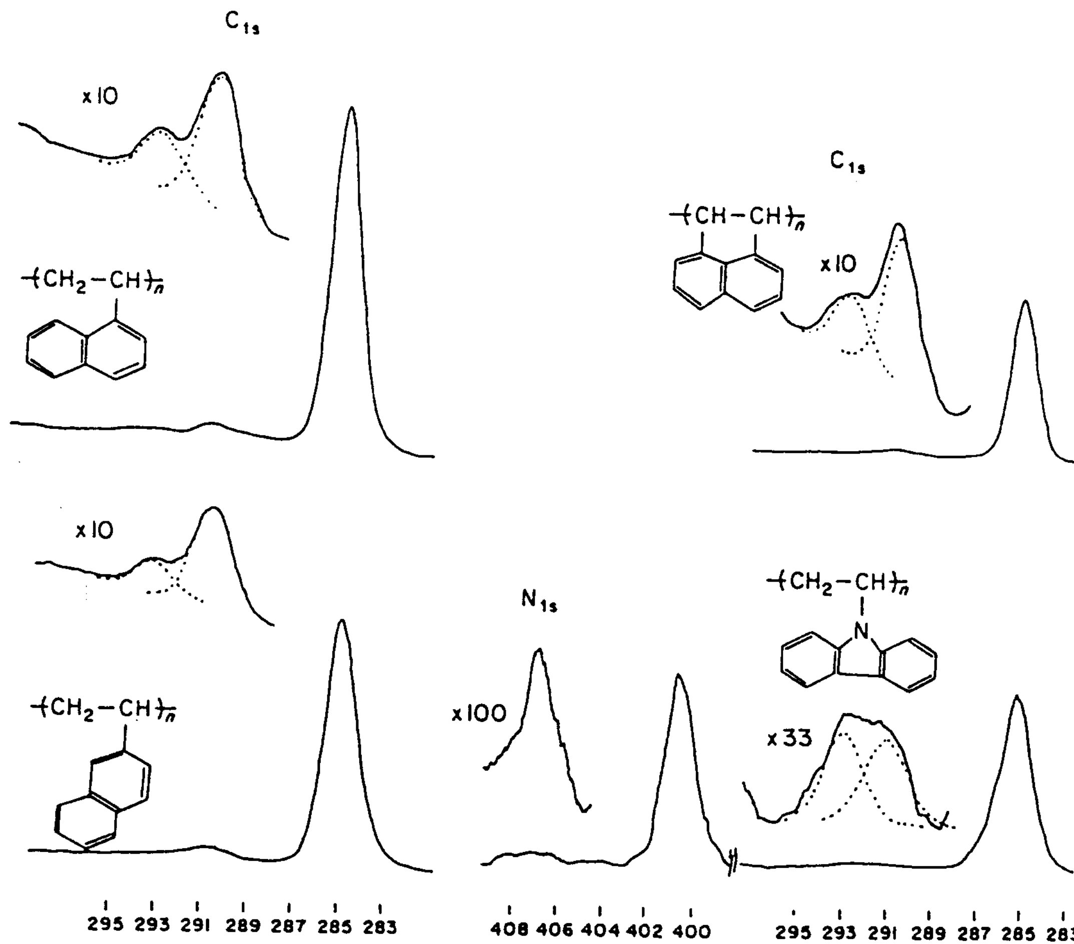

Figure 9.5 Core level spectra of poly-1- and 2-vinylnaphthalene, polyacenaphthalene and polyvinylcarbazole. (Reproduced from Clark *et al.*[39] by permission of Elsevier Science Publishers)

5.4.4 Multiplet Splitting

Occasionally see splitting of s orbitals

Occurs with photoemission from closed shell in presence of open shell

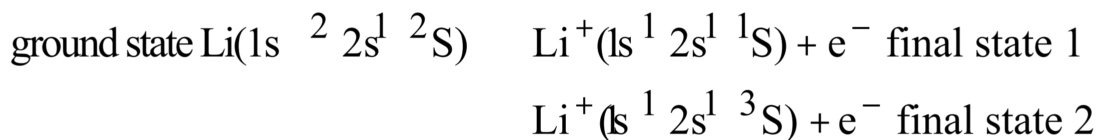

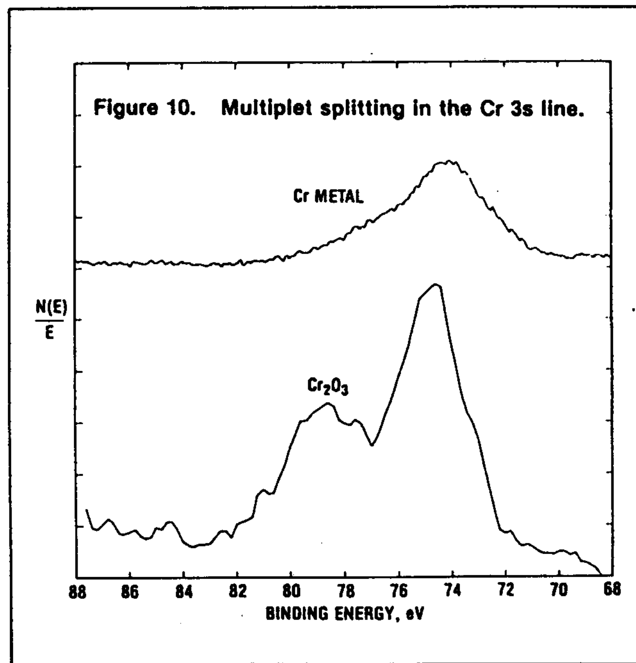

5.4.5 Extrinsic Satellites

Occur during transport of electron to surface - *discrete loss structure*

Electronic excitation (interband or plasmons (bulk or surface))

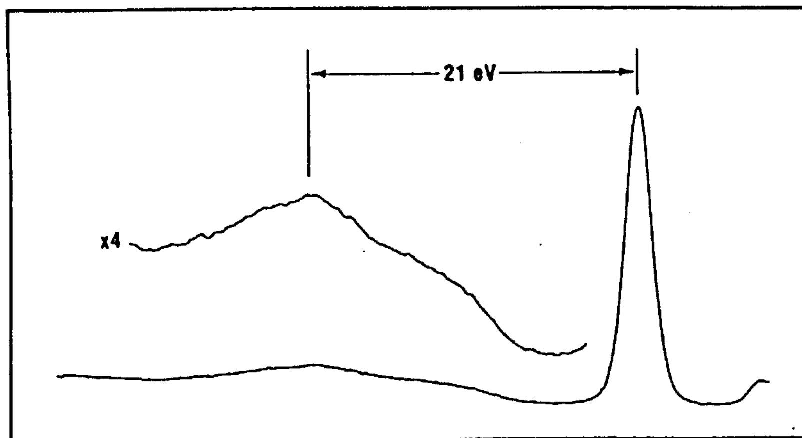

Figure 11. Energy loss envelope from the O1s line in SiO_2.

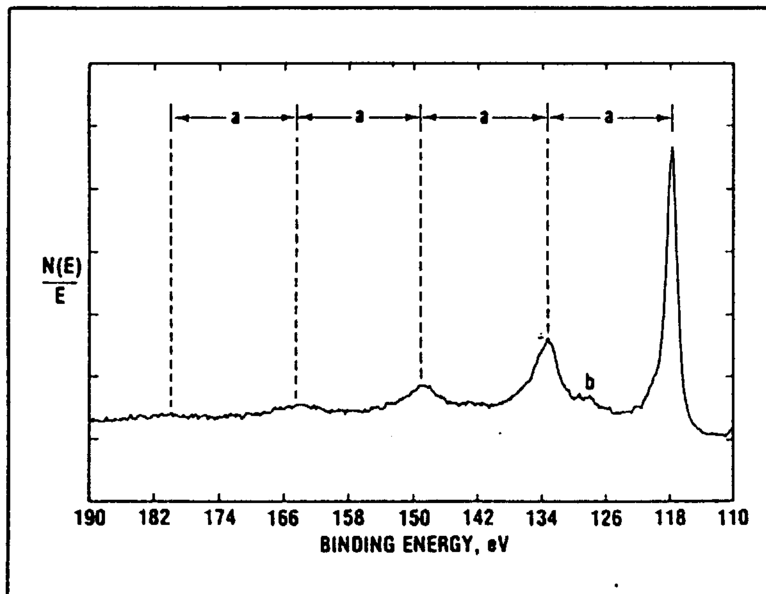

Figure 12. Energy loss (plasmon) lines associated with the 2s line of aluminum (a = 15.3eV; note surface plasmon at b).

Peak asymmetry in metals caused by small energy electron-hole excitations near E_F of metal

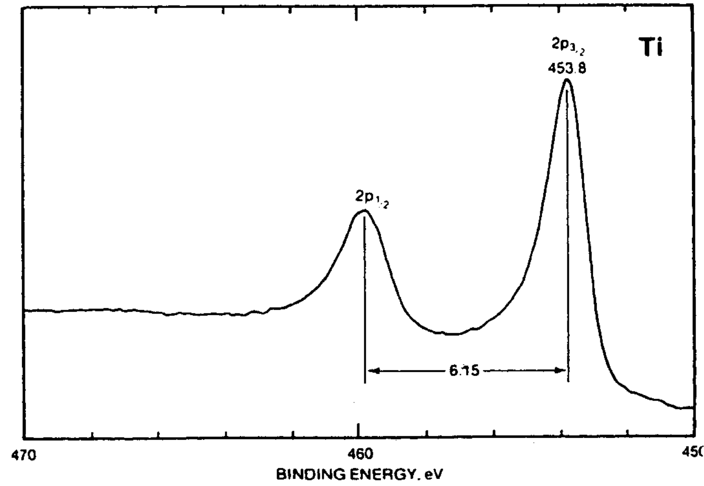

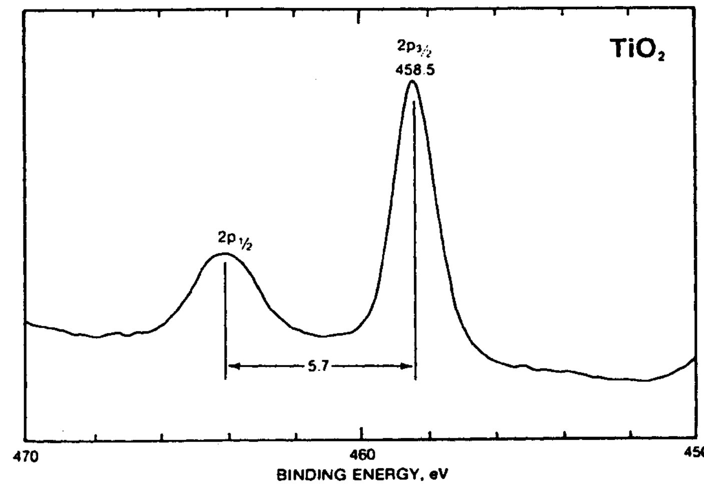

"Doniach-Sunjic" line shape

Degree of asymmetry proportional to DOS at E_F

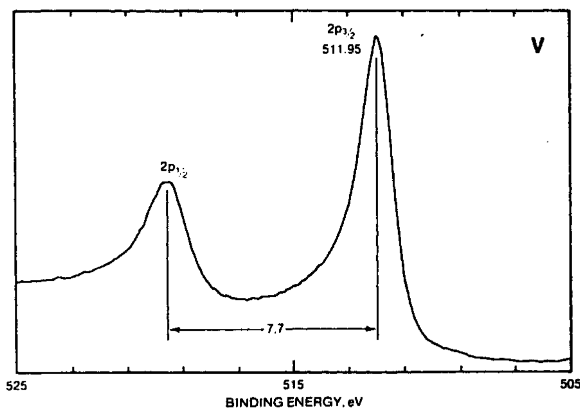

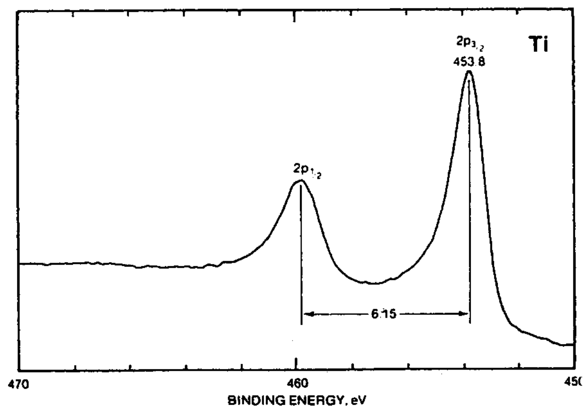

5.5 Instrumentation for XPS

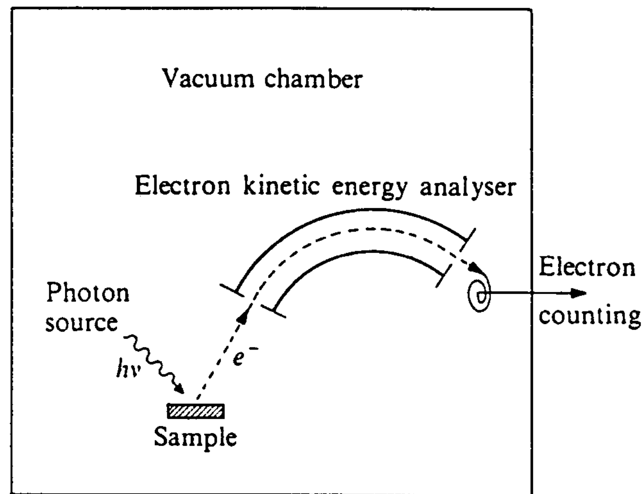

Fig. 2.2 Schematic arrangement of a photoelectron spectrometer.

X-ray source, (monochromator), sample, electron energy analyzer (monochromator), electrondetector, readout and data processing

5.5.1 X-ray Sources

Twin anode (Mg/Al) source:

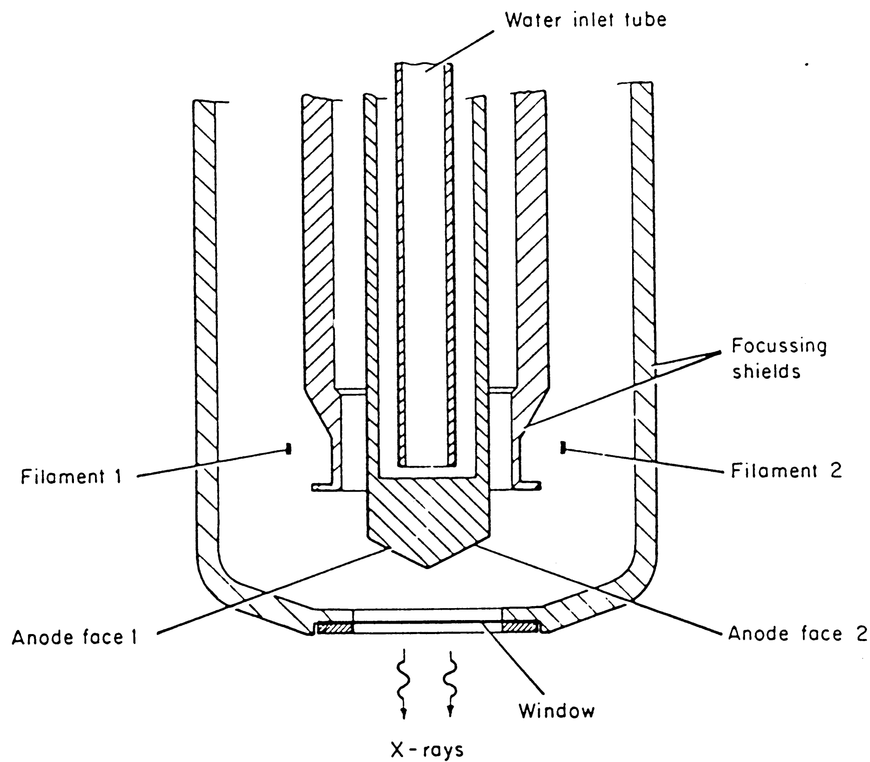

Fig. 3. Double-anode X-ray source.

TABLE 1
Some X-ray lines of use in photoelectron spectroscopy

Line	Be K	Y Mζ	Zr Mζ	Nb Mζ	Mo Mζ	Ru Mζ	Rh Mζ	C K	Ti Ll	Ti Lα	O K	Cr Lα
Energy (eV)	108.9	132.3	151.4	171.4	192.3	236.9	260.1	278	395.3	452.2	524.9	572.8
Width (eV)	5.0	0.47	0.77	1.21	1.53	2.49	4.0	6	3	3	4	3

Line	Ne Kα	Ni Lα	Cu Lα	Zn Lα	Na Kα	Mg Kα	Al Kα	Zr Lα	Ti Kα	Cr Kα	Cu Kα
Energy (eV)	849	851.5	929.7	1011.7	1041.0	1253.6	1486.6	2042	4510	5417	8048
Width (eV)	0.3	2.5	3.8	2.0	0.42	0.7	0.85	1.7	2.0	2.1	2.6

Simple, relatively inexpensive

High flux (10^{10} - 10^{12} photons$\cdot s^{-1}$)

Polychromatic

Beam size ~ 1cm

Monochromatic source:

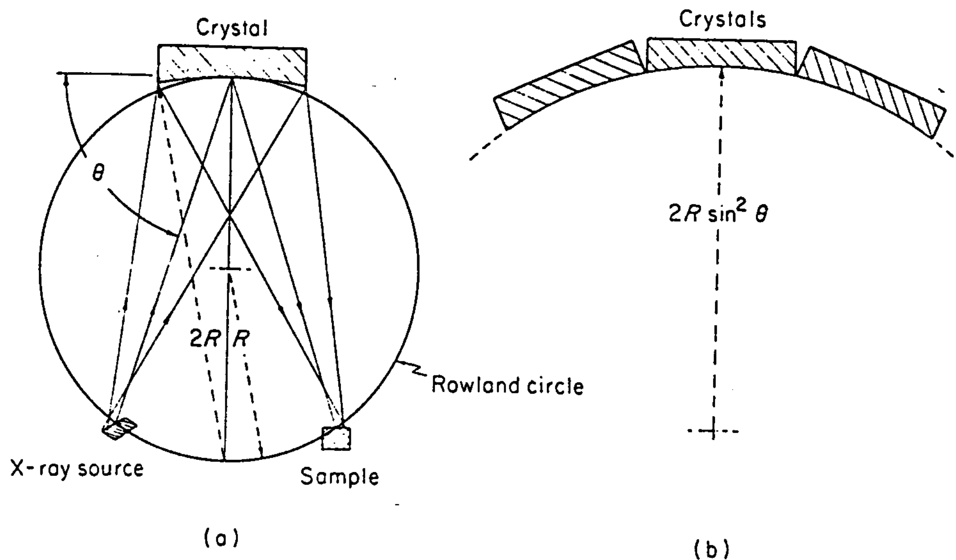

Fig. 5. X-ray monochromation (Johann approximate focusing geometry).

Diffraction from bent SiO_2 crystal - other 's focussed at different points in space

Beam size ~ 1 cm to 50 μm

Eliminates satellites, decreases FWHM of line but flux decreases at least an order of magnitude

5.5.2 Electron Energy Analyzers

Most common type of electrostatic deflection-type analyzer called the *concentric hemispherical analyzer* (CHA) or spherical sector analyzer

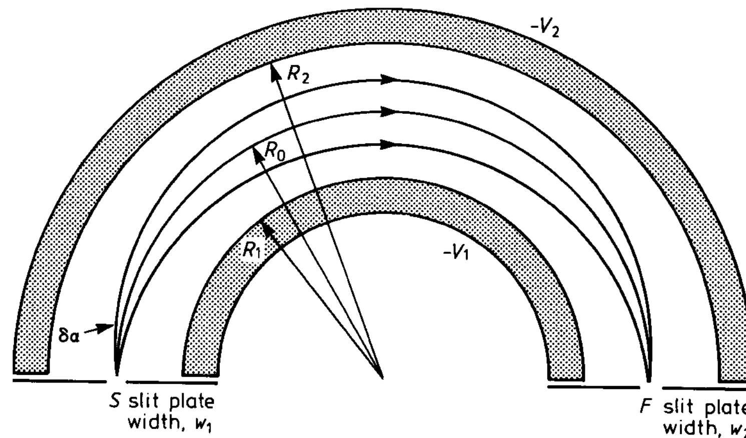

Figure 2.30 Schematic cross-section of a concentric hemispherical analyser (CHA). Two hemispheres of radii R_1 (inner) and R_2 (outer) are positioned concentrically. R_0 is the radius of the median equipotential surface. Potentials $-V_1$ and $-V_2$ are applied to the inner and outer spheres respectively, with V_2 greater than V_1. The source S is located in the entrance slit of width W_1 and the focus F in the exit slit of width W_2. The divergence of an electron entering the analyser from the ideal tangential path is $\delta\alpha$. The expression for the relationship between the energy of an electron and the difference $V_2 - V_1$ is given by equation (2.21). (Reproduced from Seah[23] by permission of Cambridge University Press. Crown © reserved)

Negative potential on two hemispheres $V_2 > V_1$

Potential of mean path through analyzer is

$$V_0 = \frac{V_1R_1 + V_2R_2}{2R_0}$$

An electron of kinetic energy $eV = V_0$ will travel a circular orbit through hemispheres at radius R_0

Since R_0, R_1 and R_2 are fixed, in principle changing V_1 and V_2 will allow scanning of electron KE following mean path through hemispheres

Total resolution of instrument is convolution of x-ray source width, natural linewidth of peak, analyzer resolution

$$FWHM_{total} = \left[\underbrace{FWHM_{x-ray}}_{0.7-1.0\,eV}{}^{2} + \underbrace{FWHM_{linewidth}}_{<0.1\,eV}{}^{2} + FWHM_{analyzer}{}^{2}\right]^{1/2}$$

Analyzer FWHM is really only one we can control

Resolution defines ability to separate closely spaced photoemission peaks (important for determining chemical shift)

$$R = \frac{E}{E}$$

$$E \quad \text{FWHM (eV)}$$

$$E = \text{KE of peak (eV)}$$

But what if we wanted uniform resolution across entire XPS spectrum? Say 0.5 eV FWHM?

At 10 eV KE, R = 0.5 / 10 = 0.05

At 1500 eV KE, R = 0.5 / 1000 = 0.0005

Easiest way is to *retard* electrons entering energy analyzer to fixed KE, called the *pass energy* E_0, so that fixed resolution applies across entire spectrum

$$\frac{E}{E_0} = \frac{s}{2R_0}$$

s = mean slit width

Decreased pass energy or increased R_0 = increased resolution (typical $FWHM_{analyzer}$ 0.1-1.0 eV)

Multi-element electrostatic lens system:

(i) Collects e^-'s of large angular distribution - larger flux

(ii) focuses e^{-}'s at entrance slit

(ii) retards electrons to pass energy

(iv) can "magnify" image of sample for small spot XPS - much easier to look at small spot with analyzer than try to produce focussed x-ray beam

Image spot can be scanned to build up 2-D chemically-resolved "image" of surface - best 5 μm

Basis of *photoemission electron microscopy* (PEEM) technique

Often coupled with *rotating anode* x-ray source to increase x-ray flux

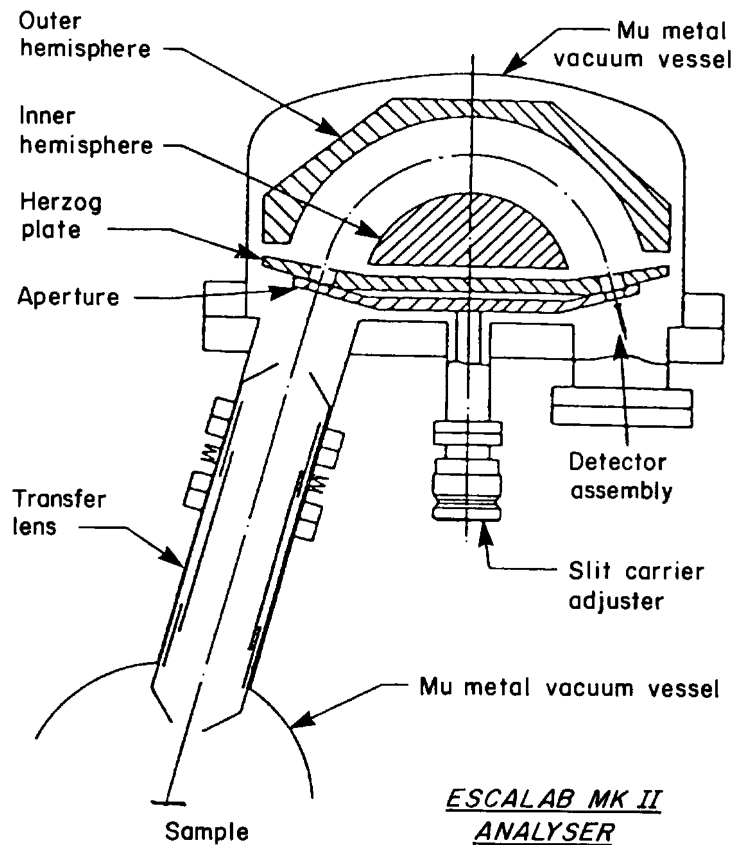

Figure 2.31 Diagram of a CHA with standard input lens systems for XPS. The lens in this case is simply a transfer lens, which transfers an image of the analysed area on the sample onto the entrance slit to the analyser. Slight magnification is also performed. Removing the sample from close proximity to the entrance slit of the analyser in this way provides much greater working space around the sample. (Reproduced from Coxon *et al.*[24] by permission of Elsevier Science Publishers)

5.6 Quantitation of XPS

Usefulness of technique depends on

(i) sensitivity (minimum detectable concentration)

(ii) quantitation (accuracy and precision)

5.6.1 Sensitivity

Basic property is probability of subshell ionization

Probability is function of initial and final state wavefunctions

$$_{i,j} = A(BE_i \; KE_j) \left| \langle \;\; _i | \mu | \;\; _f \rangle \right|^2$$

where A depends on BE of ionized core level and KE of emerging photoelectron

In effect, $_{i,j}$,measures "overlap" of initial and final state wavefunctions

Qualitative picture from radial dependence of $_i$ and wavelength of free electron:

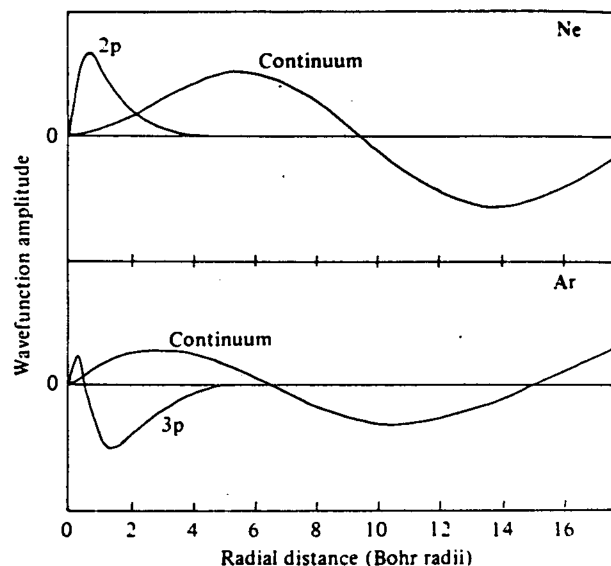

Fig. 3.21 Radial part of the 2p (Ne) and 3p (Ar) atomic wavefunctions together with the d continuum (final state) wavelengths at zero kinetic energy (i.e. at photoionisation threshold) (after Fano & Cooper, 1968).

Minimum in $_{i,j}$ about 50 eV (KE) above ionization threshold

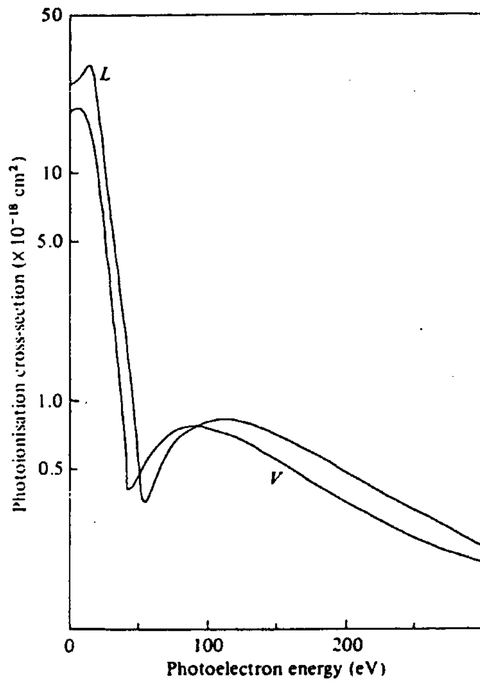

Fig. 3.22 Theoretical computation of the Ar 3p atomic photoionisation cross-section by Kennedy and Manson (1972) showing the 'Cooper minimum' around 50 eV above threshold. *L* and *V* correspond to the 'length' and 'velocity' forms of the matrix element used in the computation (cf. equation (3.12)). These computations include both d and s final states so that the minimum is not identically zero as it is in the d channel alone.

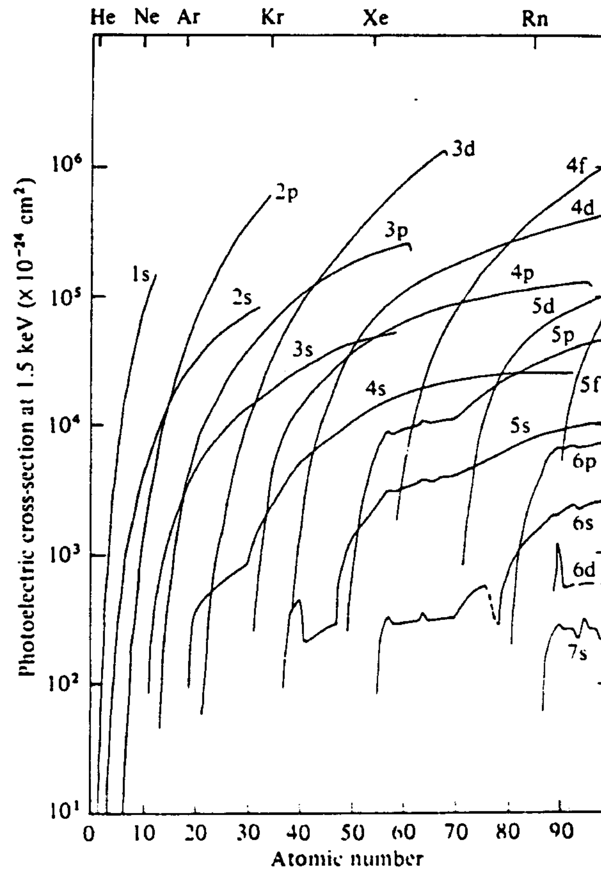

Fig. 3.16 Calculated cross-sections for photoemission from occupied levels of the elements for 1.5 keV photons (from Wertheim (1978) based on the calculated value of Scofield, 1976).

Calculations indicate maximum $_{i,j}$ is ~ 10^{-18} cm^2

If 1 ML contains 10^{15} atoms·cm^{-2}, should get about 10^{-3} photoelectron per incident photons ($10^{15} \times 10^{-18}$)

If x-ray source flux is 10^{12} photons·s^{-1}, should produce about 10^{9} electrons·s^{-1} from 1 ML

For most elements, sensitivity is 0.1-1 % ML (subnanomolar)

Observations:

$_{i,j}$ for C in CF_4, CH_4, graphite… is identical

Each subshell has different $_{i,j}$ - different sensitivity

Low Z elements have low $_{i,j}$ implies lower sensitivity

5.6.2 Quantitation

Difficult to apply calculated $_{i,j}$ directly to data (other instrumental parameters need to be included)

$$I_a = \ _{x-ray}(x,y) \times C_a(x,y,d) \times \ _{i,j}(h\ ) \times P_{no-loss}(\text{material},d) \times A_{analyzer} \times T_{analyzer}$$

$_{x\text{-ray}}$ = x-ray flux

C_a = concentration of element a

$_{i,j}$ = subshell ionization cross-section

$P_{no\text{-}loss}$ = probability of no-loss escape (IMFP)

$A_{analyzer}$ = angular acceptance of analyzer

$T_{analyzer}$ - transmission function of analyzer

Most analyses use empirical calibration constants (called *atomic sensitivity factors*) derived from standards:

$$C_a(\bar{x},\bar{y},\bar{d}) = \frac{I_{measured}}{ASF}$$

Z	Element	Subshell	ASF (Area)
3	Li	1s	0.012
4	Be	1s	0.039
5	B	1s	0.088
6	C	1s	0.205
7	N	1s	0.38
8	O	1s	0.63
9	F	1s	1.00
10	Ne	1s	1.54
11	Na	1s	2.51
12	Mg	1s	3.65
	Mg	2p	0.07
13	Al	2p	0.11
14	Si	2p	0.17
15	P	2p	0.25

Note: ASF for H, He very small - undetectable in conventional XPS!

Note: XPS spectrum will show *all* peaks for each element in same ratio

Note: Not all XPS peaks for an element same intensity (in area ratio proportional to ASF's) -choose peak with largest ASF to maximize sensitivity

Note: Sensitivity for each element in a complex mixture will vary

How to measure $I_{measured}$

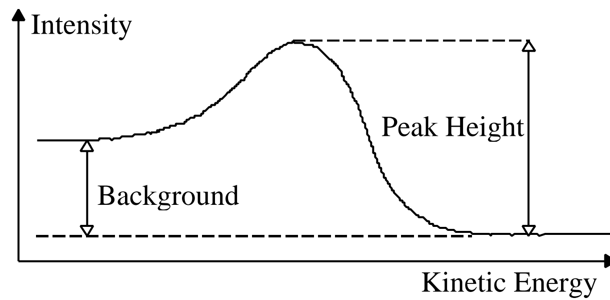

Worst

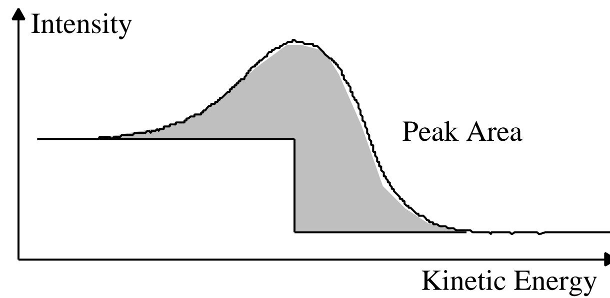

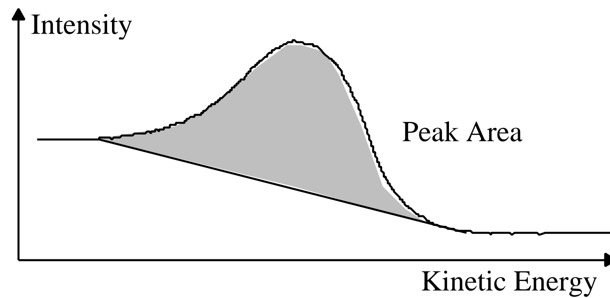

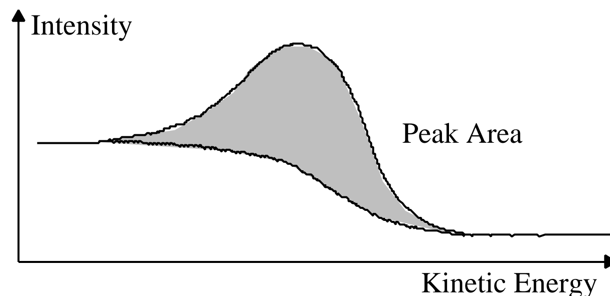

Best

Must include or correct for (i) x-ray satellites (ii) chemically shifted species (iii) shake-up peaks (iv) plasmon or other losses

Accuracy better than 15 % using ASF's

Use of standards measured on same instrument or full expression above accuracy better than 5 %

In both cases, reproducibility (precision) better than 2 %

5.6.3 Depth Information From XPS

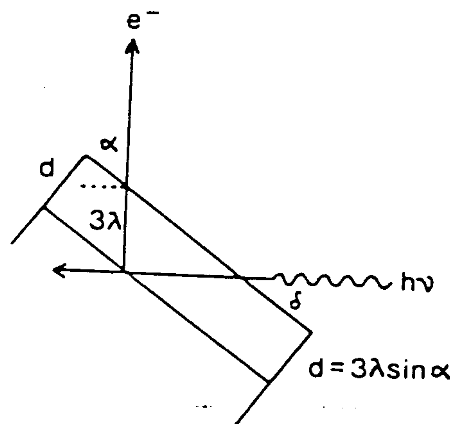

Figure 3.35 Surface sensitivity enhancemen' hy variation of the electron 'take-off' angle

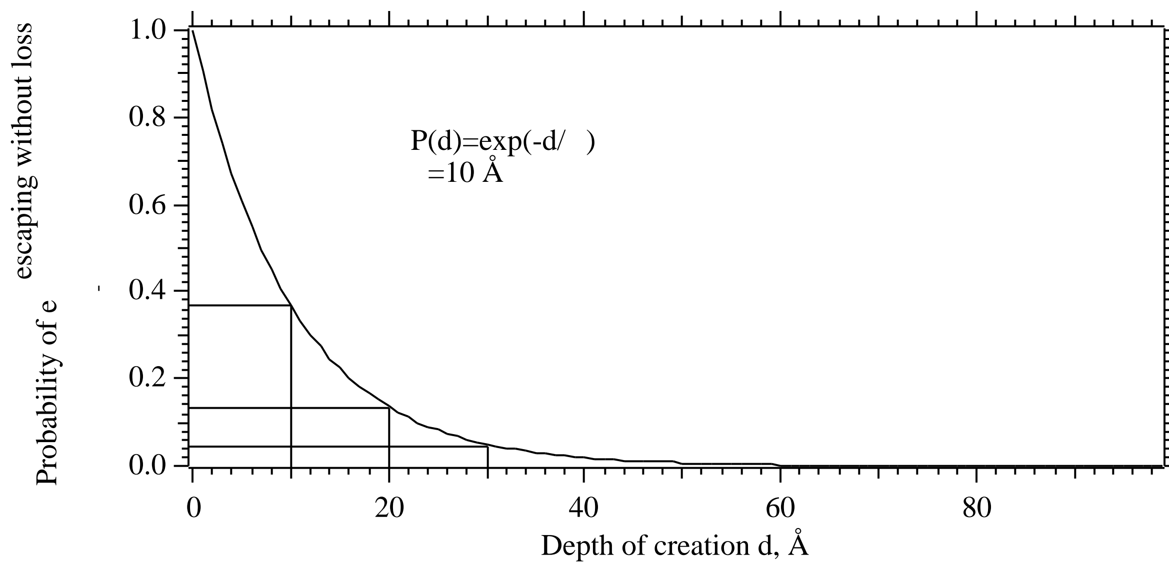

Probability that electrons can escape without losing energy is, on average IMFP, where d is called the *sampling depth* ~ 3 (for 95 % photoelectrons)

For off-normal *take-off angle* :

$$P = \exp\left(\frac{-d}{\ \sin\ }\right) \qquad P = \frac{I}{I_0}$$

$$d = -\ln(P) \quad \sin$$

$$= 3 \quad \sin$$

d decreases by a factor of 4 on going from = 90° (normal) to 15° (grazing)

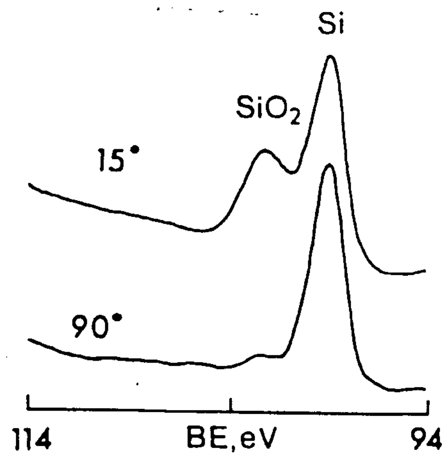

Figure 3.37 Effect of variation of take-off angle on the Si 2*p* spectrum from silicon with a passive oxide layer. Note the relative enhancement of the (surface) oxide signal at low angle (measured with respect to the surface). (After Wagner *et al.*[31])

Crude, non-destructive way of "depth profiling"

5.7 Summary

Non-destructive

Quantitative method for elemental composition - relatively straightforward using ASF's

Sensitive ~ 0.1 % ML

Chemical shifts give information about

- (i) oxidation states
- (ii) chemical environment

Extensive databases of chemical shift information

Sampling depth typically 20-100 Å

Crude depth information by changing take-off angle

BUT

Complex, expensive instrumentation (>$100,000)

Monochromatic x-ray sources have low flux

Not usually spatially sensitive

Sampling depth varies with electron KE (and material)

Spectra complicated by secondary features

- (i) x-ray satellites
- (ii) extrinsic losses
- (iii) final state effects

Surface charging in insulators shifts BE scale

Cannot detect H, He with good sensitivity